Charge separation in an acceptor–donor–acceptor triad material with a lamellar structure†

D. Rolland,[a] J. C. Brauer,[a] L. Hartmann,[a] L. Biniek,[b] M. Brinkmann,[b] N. Banerji[c] and H. Frauenrath*[a]

Linking covalently both electron donor and acceptor components is an efficient way to gain thermodynamic control over the formation of well-ordered heterojunction materials suitable for organic photovoltaics. In this context, we attached flexible polymer segments to the termini of a (perylene bisimide)–quaterthiophene–(perylene bisimide) triad. The microphase segregation of the resulting coil-rod-coil architecture served to reliably promote the formation of lamellar phases. The lamellae were oriented vertically relative to the substrate, and they could be laterally aligned by mechanical rubbing, as determined by small and wide angle X-ray scattering, transmission electron microscopy, electron diffraction and AFM. Transient absorption spectroscopy revealed that light absorption was followed by charge separation and that charge recombination was slower in thin films than for solution-phase samples, especially when longer side chains were used. Thus, this study is a first step towards reliable lamellar phase segregation in donor–acceptor materials on the route towards improved materials for organic photovoltaics.

Introduction

Research on photovoltaic devices is one of the cornerstones of solving the problems associated with the world's growing energy demand.[1,2] In this context, the use of organic materials promises a low cost production of large surface area, flexible, and light-weight devices. In organic photovoltaic materials, charge generation at the interface between an electron donor and an acceptor component as well as charge extraction towards the electrodes are the two crucial steps that determine device performance.[3–5] Therefore, both a large interface and continuous charge percolation pathways are essential for an overall efficient energy conversion. The active layer microstructure is one of the most important parameters determining device performance.[6] To this end, blending the donor and the acceptor components such that they form an interpenetrating network, called "bulk heterojunction" (BHJ), has been the most successful strategy to date.[7–9] In BHJ devices based on an electron donor polymer and a fullerene acceptor, for instance, the formation of a three-phase microstructure, including an intimately mixed phase of the two components, plays a major role for their superior efficiency.[10–13] However, the exact microstructure of BHJs is difficult to control, and they still contain large domains that result in increased exciton recombination as well as isolated domains that trap charges. Moreover, their kinetically controlled formation results in metastable morphologies that slowly undergo macrophase segregation, resulting in significantly reduced device performance over time.[9,14]

Connecting the donor and acceptor components covalently has been explored as an approach to address these issues.[15–17] For example, brush copolymers of acceptor moieties grafted onto an electron-rich polymer backbone as the donor component have been referred to as "double-cables" that transport electrons through the pendant groups and holes through the polymer backbone. Similarly, dyads or triads of small molecule donors and acceptors have been designed with the purpose of maximizing the donor/acceptor interface. The intimate mixing of the donor and acceptor moieties in such "molecular heterojunctions" is supposedly related to the mixed phase observed in polymer: fullerene BHJs. However, typical power conversion efficiencies of devices using such materials were often lower than those of devices prepared from the corresponding blends,[16–18] presumably due to better charge extraction and limited recombination assisted by larger domains of the pure components in the blends. One may conclude that covalently linking the donor and acceptor components should be complemented with the formation of nanostructures with at least one extended dimension in the

[a] Laboratory of Macromolecular and Organic Materials, Institute of Materials, Ecole Polytechnique Fédérale de Lausanne, EPFL-STI-IMX-LMOM, MXG 135, Station 12, 1015 Lausanne, Switzerland. E-mail: holger.frauenrath@epfl.ch
[b] Institut Charles Sadron, CNRS-Université de Strasbourg, 23 rue du loess, 67034 Strasbourg, France
[c] Department of Chemistry, University of Fribourg, Chemin du Musée 9, CH-1700 Fribourg, Switzerland

† Electronic supplementary information (ESI) available: Absorption spectra of all TA samples and TA spectra of individual chromophores. See DOI: 10.1039/c6tc03786k

so-called ''ordered heterojunctions''. In this context, various groups prepared donor–acceptor co-oligomers, *e.g.* dyads (AD) or triads (ADA and DAD). Hashimoto *et al.* prepared a fullerene-substituted oligothiophene that formed lamellar phases in thin films.[19] Geng *et al.* as well as Méry *et al.* prepared liquid-crystalline dyads comprising fluorene and thiophene subunits in the donor block and a perylene acceptor block that self-assembled into lamellar phases with separated donor and acceptor domains.[20–22] Tuning the band gap of the donor part and adding a flexible alkyl spacer between the donor and the acceptor to accommodate packing constraints resulted in a power conversion efficiency of 2.7%,[23] which represents one of the best values reported for a single-component organic solar cell, but is still low compared to BHJs. This problem has mostly been attributed to the lack of long-range order; as the lamellar thickness is typically on the order of only a few nanometers, an increasing number of defects will favor the charge recombination. Moreover, charge transport may be impeded by an inappropriate molecular orientation within the lamellae.

Herein, we show that terminally attaching soft polymer segments to an acceptor–donor–acceptor triad can help to obtain thin films comprising well-ordered lamellar nanostructures (Fig. 1). This ''coil-triad-coil'' architecture was deliberately chosen because microphase segregation between the coil segments and the rod-like triad core was expected to strongly favor morphologies with low-curvature interfaces, such as lamellar phases. The resulting confinement of the triad core should consequently promote a packing of the acceptor and donor segments into separate sublayers. We chose to investigate the triad (perylene bisimide)–quaterthiophene–(perylene bisimide) substituted with two poly(isobutylene) (PIB) segments of different lengths (number-average degrees of polymerization P_n = 9 and 19), which is named **PTP-9** and **PTP-19**, respectively. The triads were shown to form lamellar phases, with an ''edge-on'' orientation of the layers relative to the substrate. Rubbing and annealing served to achieve a macroscopic alignment of the lamellar phases. In this context, the longer polymer segments of **PTP-19** helped to prevent the lamellae to attain a face-on orientation that was observed in the case of **PTP-9** after rubbing and annealing. Femtosecond-resolved transient absorption (TA) studies confirmed that light absorption was followed by charge separation and that the lifetime of the charges was increased in thin films in comparison to solution-phase samples. In this way, our study represents a first step towards reliable lamellar phase segregation in donor–acceptor materials on the route towards improved materials for organic photovoltaics.

Experimental

Instrumentation and methods

Mass spectrometry. Mass spectra were recorded at the Mass Spectrometry Service of EPFL on a Waters Q-TOF Ultima for ESI-TOF, a Shimadzu Biotech AXIMA Performance for MALDI-TOF, or a Thermo Scientific LTQ FT-ICR MS for APPI.

NMR spectroscopy. ^{1}H and ^{13}C NMR spectroscopy studies were carried out on a Bruker Avance 400 or 600 spectrometer operating at frequencies of 400.13 MHz or 600.13 MHz for ^{1}H nuclei, and at 100.62 MHz or 150.91 MHz for ^{13}C nuclei, respectively. Deuterated solvents were purchased from Cambridge Isotope Laboratories, Inc. The spectra were calibrated to the respective residual proton peaks of the deuterated solvents (^{1}H NMR: 7.26 ppm for $CDCl_3$, 2.50 ppm for DMSO-d_6, and 6.00 ppm for TCE-d_2; ^{13}C NMR: 77.00 ppm for $CDCl_3$ and 40.45 ppm for DMSO-d_6). Data are reported as follows: s = singlet, d = doublet, t = triplet, q = quartet, and m = multiplet. Coupling constants J are reported in Hz. The coupling patterns and coupling constants were evaluated using Mestrenova NMR data processing.

SAXS and WAXS. Measurements were performed in collaboration with Dr Sandor Balog at the Adolphe Merklé Institute, Fribourg, with a NanoMax-IQ camera (Rigaku Innovative Technologies, Auburn Hills, USA). The samples were kept in vacuum at room temperature during the measurements. The scattering data were presented as a function of the scattering vector modulus $q = 4\pi/\lambda \sin(\theta/2)$, where θ is the scattering angle and λ is the photon wavelength.

Thin film rubbing, transmission electron microscopy, and electron diffraction. Thin film samples were prepared by doctor-blading from sample solutions in *ortho*-dichlorobenzene (c = 5 mg mL^{-1}) on a clean glass substrate maintained at 170 °C. The thin films were subsequently rubbed with a microfiber cloth in an inert atmosphere in a glove box (Plas Labs Inc.). The rubbing apparatus consisted of a rotating cylinder (4 cm diameter)

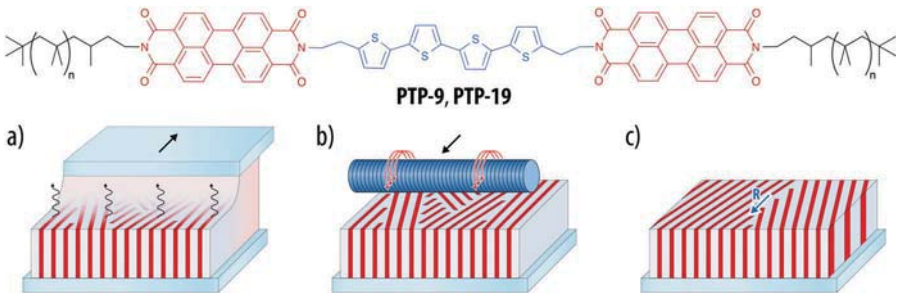

Fig. 1 Molecular structure of the polymer-substituted donor–acceptor–donor triads and preparation of thin films. (a) Thin films of **PTP-9** or **PTP-19** (n = 9 or 19, respectively) prepared by doctor blading exhibiting a lamellar phase with an ''edge-on'' orientation of the lamellae relative to the substrate and with different lateral orientations. (b) Mechanical rubbing and annealing resulting in (c) a macroscopic alignment of the lamellar phase parallel to the rubbing direction.

covered by a microfiber cloth. The rubbing was performed by applying the rotating cylinder with 2 bar pressure on the translating sample holder (1 cm s^{-1}) such that it took accordingly 5 s to align a 5 cm long film. The sample holder was heated at different temperatures in the range of 25–200 °C during the rubbing process and the temperature was allowed to equilibrate for 1–2 min before rubbing. One rubbing cycle corresponded to a rubbing length (*i.e.* the length of the rubbing tissue applied at a given point of the sample) of 50 cm. The films were finally annealed in a Linkam LTS420 hotplate under a nitrogen atmosphere at 300 °C for 5 min and cooled to room temperature at a rate of 10 °C min^{-1}. Areas for TEM analysis were identified by optical microscopy (Leica DMR-X microscope). The thin film samples for TEM imaging were coated with a thin amorphous carbon film and removed from the glass substrate by floating on a diluted aqueous HF solution (10 wt%) with subsequent recovery on TEM copper grids. TEM imaging was performed in bright field, high resolution and diffraction modes using a CM12 Philips microscope equipped with a MVIII (Soft Imaging System) charge coupled device camera.

Atomic force microscopy. Thin films of triads **PTP-9** and **PTP-19** were analyzed in tapping mode using a Nanoscope IIIa (Veeco Instruments Inc., Santa Barbara, USA) instrument at room temperature in air. Cantilevers with a resonance frequency on average of f_0 = 325 kHz and k = 40 N m^{-1} were used. Scan rates between 0.5 and 2 Hz were applied; the image resolution was 512 × 512 pixels.

Transient absorption spectroscopy. Transient absorption (TA) spectra were recorded by femtosecond pulsed laser pump–probe spectroscopy. The sample solutions were placed in a 1 mm cell and constantly bubbled with argon gas to provide stirring and prevent degradation by oxygen. For thin film measurements, the samples were mounted on a custom-built sample chamber filled with argon to avoid sample degradation. The probe beam consisted of a white light continuum (350–750 nm), generated by passing a part of the 780 nm amplified 1 kHz Ti:sapphire output (Clark-MXR, CPA-2001) through a 5 mm CaF_2 plate. The remaining intensity of the fundamental beam was removed by a 750 nm low-pass filter. Excitation pulses at 390 nm were generated by frequency doubling of the fundamental of the laser. Excitation pulses at 540 nm were generated in a custom-built NOPA. The probe intensity was always less than the pump intensity, and the probe spot size was chosen to be much smaller than the pump spot size to allow for a homogeneous excitation over the probed area. The pump pulses were delayed with respect to the probe pulses using a computerized translation stage. The probe pulses were split before the sample by means of a beam splitter into a signal (transmitted through the sample) and a reference beam. The probe signal and reference beams were detected separately using a pair of 163 mm spectrographs (Princeton Instruments, SpectraPro 2500i) equipped with 512 × 58 pixel back-thinned CCDs (Hamamatsu S07030-0906) and assembled by Entwicklungsbüro Stresing, Berlin. The pump beam was chopped up into half the amplifier frequency to improve the sensitivity of the set-up. The transmitted intensity of the probe beam was recorded shot by shot and corrected for laser intensity fluctuations using the reference beam. The transient spectra were averaged at each delay until the desired signal-to-noise ratio was achieved (3000 times). To avoid polarization effects, the relative polarization of the probe and pump pulses was set to the magic angle. All spectra were corrected for the chirp of the white-light probe.

Synthetic procedures

***N*-Poly(isobutene)-yl perylene-9,10-di(propylcarboxylate)-3,4-dicarboximide 3a.** A slurry of perylene-3,4:9,10-tetracarboxylic dianhydride **1** (13.0 g, 33.1 mmol), 1-propanol (20 mL, 265 mmol), and DBU (20 mL, 133 mmol) in dry DMF (130 mL) was stirred for 16 h at room temperature in an inert atmosphere. The slurry became a clear solution after 1 h. Dry THF (80 mL) and then a solution of PIB–NH_2 **2a** (20 g, 16.6 mmol) in dry THF (70 mL) were added slowly to the reaction mixture. The solution was stirred vigorously for 3 d, treated with 1-bromopropane (24 mL, 265 mmol), stirred for another 16 h, and finally poured into a 1 M aqueous HCl solution. The slurry was extracted three times with DCM. The combined organic phases were washed with a 1 M aqueous HCl solution, two times with a saturated aqueous NaCl solution, and finally dried over Mg_2SO_4. The solvent was removed *in vacuo*, and the residue (about 38 g) was purified by column chromatography (5 L SiO_2, DCM) to afford pure **3a** as a red sticky solid (12.7 g, 45%). ^{1}H NMR (400.13 MHz, $CDCl_3$): δ = 0.65–1.80 (m, 132H, aliphatic *H*), 1.85 (sex, 2H, $COOCH_2CH_2CH_3$) 4.13–4.26 (m, 2H, CH_2-N), 4.32 (t, 4H, $COOCH_2$), 8.06 (m, 2H, Ar*H*), 8.35 (m, 4H, Ar*H*), 8.53 (m, 2H, Ar*H*).

***N*-Poly(isobutene)-yl perylene-9,10-di(propylcarboxylate)-3,4-dicarboximide 3b.** A slurry of perylene-3,4:9,10-tetracarboxylic dianhydride **1** (0.55 g, 1.40 mmol), 1-propanol (0.84 mL, 11.2 mmol), and DBU (0.84 mL, 5.6 mmol) in dry DMF (8 mL) was stirred for 16 h at room temperature in an inert atmosphere. The slurry became a clear solution after 1 h. Dry THF (6 mL) and then a solution of PIB–NH_2 **2b** (11.0 g, 9.13 mmol) in dry THF (5 mL) were added slowly to the reaction mixture. The solution was stirred vigorously for 3 d, treated with 1-bromopropane (1.02 mL, 11.2 mmol), stirred for another 16 h, and finally poured into a 1 M aqueous HCl solution. The slurry was extracted three times with DCM. The combined organic phases were washed with a 1 M aqueous HCl solution, two times with a saturated aqueous NaCl solution, and finally dried over Mg_2SO_4. The solvent was removed *in vacuo*, and the residue (about 1.21 g) was purified by column chromatography (150 mL SiO_2, DCM) to afford pure **3b** as a red sticky solid (0.43 g, 60%). ^{1}H NMR (400.13 MHz, $CDCl_3$): δ = 0.65–1.80 (m, 191H, aliphatic *H*), 1.85 (sex, 4H, $COOCH_2CH_2CH_3$) 4.13–4.26 (m, 2H, CH_2-N), 4.32 (t, 4H, $COOCH_2$), 8.06 (m, 2H, Ar*H*), 8.34 (m, 4H, Ar*H*), 8.53 (m, 2H, Ar*H*).

***N*-Poly(isobutene)-yl perylene-9,10-di(carboxylic anhydride)-3,4-dicarboximide 4a.** *N*-Poly(isobutene)-yl perylene-9,10-di(propylcarboxylate)-3,4-dicarboximide **3** (10.14 g, 8.20 mmol) and *p*-toluene sulfonic acid monohydrate (15.6 g, 82.0 mmol) were dissolved in toluene (150 mL), and the resulting solution was stirred for 16 h at 95 °C. After cooling to room temperature, the reaction mixture was poured into MeOH (1.5 L), and the resulting slurry was stirred for 2 h. The red precipitate was filtered off, washed with MeOH, taken up in THF (200 mL), and

re-precipitated into MeOH (2 L) to afford pure **4a** as a red sticky solid (8.77 g, 94%). ^{1}H NMR (400.13 MHz, $CDCl_3$, 120 °C): δ = 0.65–1.85 (m, 123H, aliphatic *H*), 4.17–4.29 (m, 2H, C*H*$_2$-N), 8.58–8.72 (m, 8H, Ar*H*).

***N*-Poly(isobutene)-yl perylene-9,10-di(carboxylic anhydride)-3,4-dicarboximide 4b.** *N*-Poly(isobutene)-yl perylene-9,10-di-(propylcarboxylate)-3,4-dicarboximide **3** (300 mg, 178 μmol) and *p*-toluene sulfonic acid monohydrate (169 mg, 890 μmol) were dissolved in toluene (15 mL), and the resulting solution was stirred for 16 h at 95 °C. After cooling to room temperature, the reaction mixture was diluted in DCM, washed with water, and dried. The red solid was taken up in THF and re-precipitated into MeOH to afford pure **4b** as a red sticky solid (277 mg, 98%). ^{1}H NMR (400.13 MHz, $CDCl_3$, 120 °C): δ = 0.65–1.85 (m, 231H, aliphatic *H*), 4.17–4.29 (m, 2H, C*H*$_2$-N), 8.58–8.72 (m, 8H, Ar*H*).

PIB$_9$–PBI–T$_4$–PBI–PIB$_9$ PTP-9. 5-5‴-Bis(2-amino-ethyl)-2,2′:5′,2″:5″,2‴-quaterthiophene dihydrochloride (150 mg, 360 μmol), perylene-9,10-dicarboxylic anhydride-3,4-dicarboximide-*N*-(poly-isobutyl) **4a** (858 mg, 756 μmol), and $Zn(OAc)_2$ (132 mg, 720 μmol) were dissolved in quinoline (100 mL). The resulting solution was stirred for 16 h at 175 °C. The reaction mixture was subsequently cooled to room temperature and then poured into MeOH (800 mL). After stirring for 4 h, the dark red precipitate was filtered off, redissolved in THF (50 mL), and reprecipitated into MeOH (500 mL). The obtained residue was then redissolved in DCM containing SiO_2 (100 mL), and the slurry was evaporated to obtain the crude product dry-loaded onto SiO_2 for the subsequent column chromatography (200 mL SiO_2, DCM/MeOH 10 : 1, then pure THF). A final precipitation from THF to MeOH afforded pure **PTP-9** as a red sticky solid (54 mg, 42%). ^{1}H NMR (400.13 MHz, TCE-d$_2$, 120 °C): δ = 0.80–2.00 (m, 236H, aliphatic *H*), 3.35–3.42 (m, 4H, C*H*$_2$-N), 4.25–4.38 (m, 4H, quaterthiophene-CH$_2$C*H*$_2$-N), 4.56–4.65 (m, 4H, quaterthiophene-C*H*$_2$CH$_2$-N), 8.65–8.80 (m, 16H, perylene Ar*H*). HRMS (MALDI): calcd for $C_{158}H_{214}N_4O_8S_4^+$ ([M + Na]$^+$): 2447.5270; found: 2449.819.

PIB$_{19}$–PBI–T$_4$–PBI–PIB$_{19}$ PTP-19. 5-5‴-Bis(2-amino-ethyl)-2,2′:5′,2″:5″,2‴-quaterthiophene dihydrochloride (15 mg, 36 μmol), perylene-9,10-dicarboxylic anhydride-3,4-dicarboximide-*N*-(poly-isobutyl) **4b** (120 mg, 76 μmol), and $Zn(OAc)_2$ (13 mg, 72 μmol) were dissolved in quinoline (20 mL). The resulting solution was stirred for 16 h at 175 °C. The reaction mixture was subsequently cooled to room temperature and then poured into MeOH (150 mL). After stirring for 4 h, the dark red precipitate was filtered off, redissolved in THF (20 mL), and reprecipitated into MeOH (150 mL). The obtained residue was then redissolved in THF containing SiO_2 (10 mL), and the slurry was evaporated to obtain the crude product dry-loaded onto SiO_2 for the subsequent column chromatography (50 mL SiO_2, DCM/MeOH 10 : 1, then pure THF). A final precipitation from THF to MeOH afforded pure **PTP-19** as a red sticky solid (54 mg, 42%). ^{1}H NMR (400.13 MHz, TCE-d$_2$, 120 °C): δ = 0.75–1.95 (m, 358H, aliphatic *H*), 3.35–3.42 (m, 4H, C*H*$_2$-N), 4.26–4.35 (m, 4H, quaterthiophene-CH$_2$C*H*$_2$-N), 4.56–4.65 (m, 4H, quaterthiophene-C*H*$_2$CH$_2$-N), 8.65–8.80 (m, 16H, perylene Ar*H*).

Results and discussion

Synthesis and steady-state spectroscopy

The synthesis of **PTP-9** and **PTP-19** started from perylene bisanhydride **1** that was first coupled to poly(isobutylene) amines PIB$_9$–NH$_2$ **2a** and PIB$_{19}$–NH$_2$ **2b**, respectively (Scheme 1). Due to solubility reasons, however, a simple statistical coupling of one equivalent of poly(isobutylene) amine to perylene bisanhydride yielded exclusively the symmetrically disubstituted product. In order to circumvent this issue, **1** was first reacted with propanol in the presence of a strong base in DMF.[24,25] The resulting partially esterified intermediate became well soluble in DMF and was then statistically reacted *in situ* with substoichiometric amounts of poly(isobutylene) amine **2a** or **2b**. Addition of bromopropane finally yielded the unsymmetric perylene diesters **3a** and **3b**, respectively. The ester functions were subsequently cleaved under acidic conditions, and the resulting perylene monoanhydrides **4a** and **4b** were coupled to 2,5‴-bis(2-amino-ethyl)-5,2′:5′,2″:5″,2‴-quaterthiophene[26] in quinoline at 175 °C, yielding the desired triads **PTP-9** and **PTP-19** (Fig. S1, ESI†).

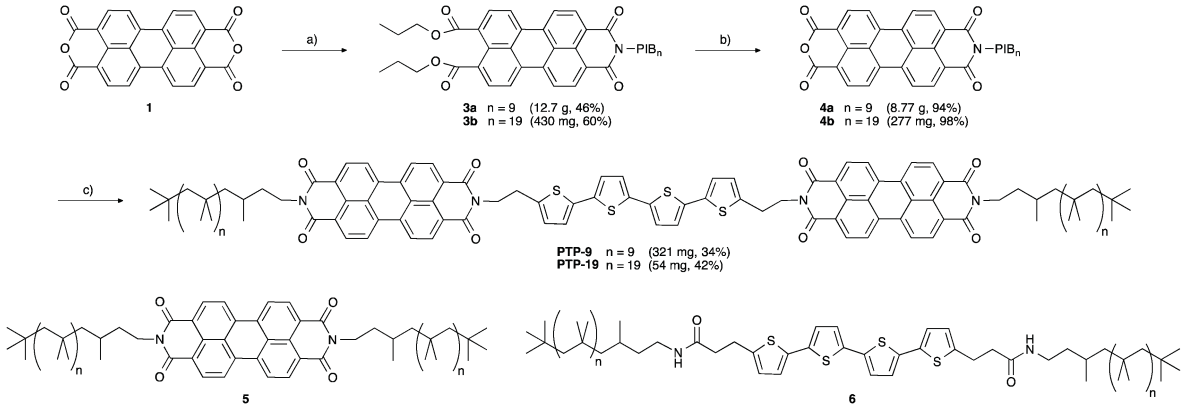

Scheme 1 Synthesis of poly(isobutylene)-substituted triads **PTP-9** and **PTP-19**. Reagents and conditions: (a) (i) propanol, DBU, DMF, r.t., 16 h; (ii) PIB–NH$_2$ **2a** or **2b**, THF, r.t., 3 d; (iii) bromopropane, r.t., 16 h; (b) TsOH·H$_2$O, toluene, 95 °C, 16 h; (c) 2,5‴-bis(2-amino-ethyl)-5,2′:5′,2″:5″,2‴-quaterthiophene, $Zn(OAc)_2$, quinoline, 175 °C, 16 h.

Moreover, the poly(isobutylene)-substituted perylene bisimide **5** and the quaterthiophene **6** were prepared as reference compounds.[26,27] Molecularly dispersed solutions of **PTP-9** and **PTP-19** in *o*-dichlorobenzene (c = 25 μmol L^{-1}) were obtained at 100 °C. The steady-state UV/vis absorption spectra of these solutions at 100 °C (Fig. 2a) resembled a superposition of the absorption spectra of perylene bisimide **5** and quaterthiophene **6**, confirming that no significant electronic coupling occurred between both chromophores. While the solutions remained optically clear upon cooling, both blue-shifted H-bands and red-shifted J-bands appeared in the absorption spectra, indicating that the triads started to form spectroscopic aggregates. The H-bands of the perylene bisimide chromophores presumably overlapped with the quaterthiophene absorption, so that the contribution of the latter became impossible to distinguish.

Thin film samples of **PTP-9** and **PTP-19** were prepared on glass slides by doctor-blading from *o*-dichlorobenzene solutions (c = 5 mg mL^{-1}) at 180 °C. As no thermal transitions were observed in differential scanning calorimetry up to temperatures of 380 °C except for the poly(isobutylene) glass transition at around −60 °C, absorption spectra of the thin films were recorded over a temperature range from 25 °C to 300 °C (Fig. 2b). The shape of the spectra was retained up to a temperature of about 175 °C, with only a slight intensity decrease of the absorption at 467 nm. Above that temperature, the bands at 467 nm and 610 nm disappeared, and new maxima at 509 nm as well as at 542 nm emerged that resemble the vibronic fine structure of non-aggregated perylene chromophores. For this reason, although no melting transition had been observed in DSC measurements, we chose to subject the film samples to further treatment at temperatures above 175 °C.

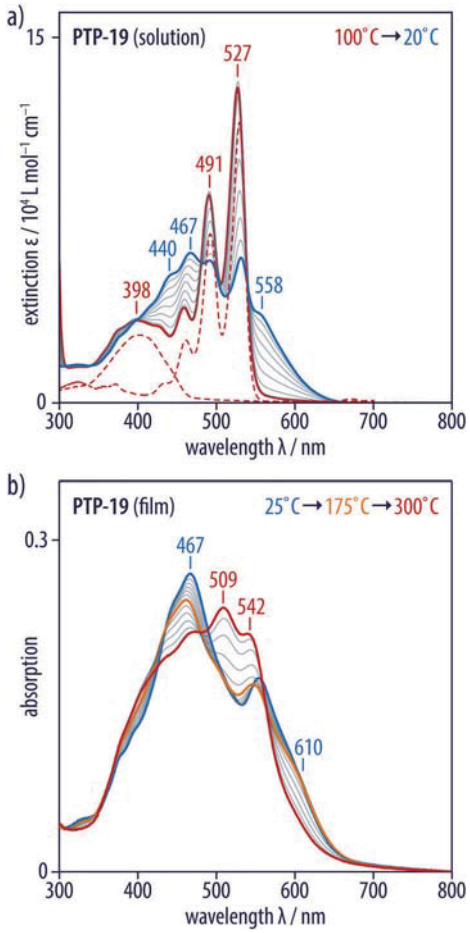

Fig. 2 (a) The UV/vis absorption spectrum of **PTP-19** in *o*-dichlorobenzene (c = 25 μmol L^{-1}) at 100 °C (red) resembling a superposition of the contributions of perylene bisimide and quaterthiophene chromophores, as seen from a comparison to the UV/vis spectra of molecularly dispersed solutions of the reference compounds **5** and **6** (red, dashed). Upon cooling the solutions from 100 °C to 20 °C (blue; in steps of 10 °C), the triad formed spectroscopic aggregates, showing both H and J bands of the perylene bisimide. (b) The shape of the UV/vis absorption spectra of **PTP-19** in thin films remained almost unchanged upon heating from 25 °C (blue) to 175 °C (orange; in steps of 25 °C), but underwent significant changes upon further heating to 300 °C (red; in steps of 25 °C).

Alignment and thin film morphology

In order to produce macroscopically aligned samples, the thin film samples were subjected to mechanical rubbing with a rotating cylinder covered with a cloth at a substrate temperature of 200 °C in an inert atmosphere, followed by thermal annealing at 300 °C. According to the evolution of the dichroic ratio *versus* rubbing temperature (Fig. S2, ESI†), the best orientation was observed for a rubbing temperature close to 200 °C. After the alignment procedure, the thin films were found to be strongly birefringent as determined by polarized optical microscopy, with a uniform transmission maximum across the film when the crossed polarizers were oriented at 45° relative to the rubbing direction, and a total extinction across the whole sample at 0°/90° orientation (Fig. 3a). This finding was an indication of a homogeneous alignment over the length scale of the thin film sample of 1 × 5 cm. Moreover, polarized UV/vis absorption spectroscopy of **PTP-19** and **PTP-9** revealed dichroic ratios of 2.7 and 6.4 for the main absorption band at 558 nm, respectively, with a maximum absorption when the polarizer was oriented parallel to the rubbing direction (Fig. 3b). Since the transition dipole in the PBI chromophore is oriented along the molecular long axis,[28] the PBI molecules are hence oriented with their long axis, on average, parallel to the rubbing direction *R*. We confirmed the presence of lamellar nanostructures in the rubbed thin films with macroscopically aligned lamellae oriented normal to the substrate plane by a combination of small-angle X-ray scattering (SAXS), wide-angle X-ray scattering (WAXS), transmission electron microscopy (TEM), and atomic force microscopy (AFM). SAXS measurements on bulk samples of **PTP-9** exhibited a series of peaks with a ratio of reciprocal spacings of $q_1 : q_2 : q_3 = 1 : 2 : 3$, as is characteristic of lamellar phases (Fig. 4). For **PTP-19**, a ratio of $q_1 : q_2 : q_3 : q_4 = 1 : 2 : 3 : 4$ was observed, with the q_3 reflection hidden in the flank of the next reflection. The main reflections corresponded to lamellar periodicities of 6.40 nm (**PTP-9**) and 7.47 nm (**PTP-19**), which are significantly smaller than the respective molecular lengths of 10 and 13 nm, even considering that the poly(isobutylene) segments assumed their preferred 8_3 helical conformation.[29]

Since the larger cross-sectional areas of poly(isobutylene)s (36 $Å^2$)[29] as compared to the perylene bisimide (28 $Å^2$)[22] and

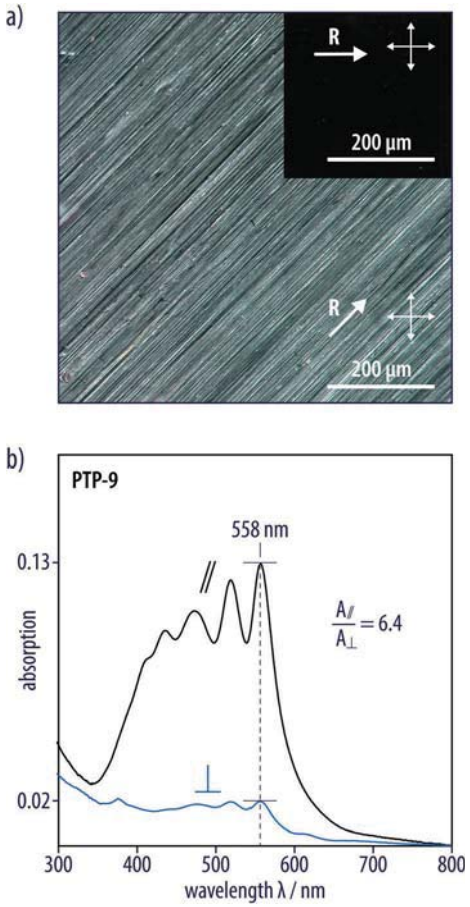

Fig. 3 Aligned thin films of **PTP-9** showing birefringence and dichroism. (a) Polarized optical micrographs showing a strong birefringence when the rubbing direction *R* (white arrow) was oriented at 45° relative to the crossed polarizers, and no transmission when the rubbing direction *R* was perpendicular to one of the polarizers (inset). (b) Polarized UV/vis spectra revealing an absorption maximum at 558 nm with a maximum intensity when the incident light was parallel to the rubbing direction.

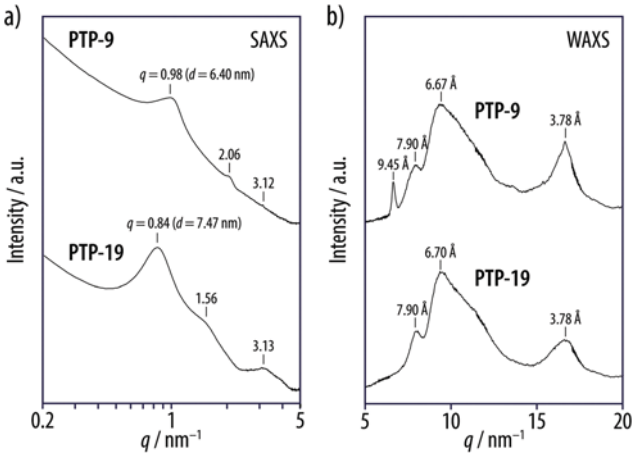

Fig. 4 X-ray scattering of bulk samples of **PTP-9** and **PTP-19** revealing lamellar structures in the bulk. (a) In the small-angle region, a reciprocal spacing ratio of $q_1 : q_2 : q_3 = 1 : 2 : 3$ and a periodicity of 6.4 nm for **PTP-9**, as well as of $q_1 : q_2 : q_3 : q_4 = 1 : 2 : 3 : 4$ and 7.5 nm for **PTP-19** are observed. (b) In the wide-angle region, the reflection at 3.78 Å is assigned to π–π stacking, and additional peaks corresponding to 7.9 and 6.7 Å are observed, of which the latter comprised at least the broad reflection associated with the short range order of poly(isobutylene). The reflection at 9.45 Å for **PTP-9** probably originates from impurities.

quaterthiophene segments (21 Å^2)[30] render an interdigitation of the former unlikely, this finding implies that different segments assume tilt angles relative to the layer normal. WAXS measurements revealed reflections at 3.8 and 7.9 Å, which were attributed to π–π stacking and a packing distance typically observed for perylenes, respectively. A broad reflection was observed with an apparent maximum at 6.7 Å, which comprised the broad reflection associated with the short range order of poly(isobutylene) at around 6 Å.[31,32]

A further investigation of the thin film nanostructure by transmission electron microscopy (TEM) confirmed the formation of lamellar phases. After doctor blading but before annealing, the thin films of both **PTP-9** and **PTP-19** showed stripes with a periodicity of about 7 nm (Fig. 5a and b). Since this periodicity was in excellent agreement with the SAXS data, one can unambiguously attribute the observed stripes to lamellae oriented normal to the substrate, with the contrast in the bright-field TEM images originating from domains of the triad cores containing the sulfur atoms *versus* the peripheral isobutylene layers. TEM however did not allow distinguishing the central quaterthiophene block from the two perylene bisimide blocks. For **PTP-19** with its longer polymer side chains, these stripes were locally aligned with a higher degree of long range order, indicative of aligned smectic lamellar phases.

After rubbing and annealing of the samples, the lamellae of **PTP-19** became macroscopically aligned parallel to the rubbing direction (Fig. 5d) and exhibited an azimuthal orientation distribution of about ±20°. In the case of **PTP-9**, the lamellar orientation of the rubbed films changed after annealing at 300 °C, from an ''edge-on'' to a ''face-on'' orientation. The change in orientation of the lamellae is visible in the bright-field TEM images showing a characteristic terraced morphology (Fig. 5c). A similar reorientation and its dependence on the molecular length had previously been observed for other perylene bisimide derivatives[33] as well as for simple polystyrene–polyisoprene block copolymers,[34,35] where it had been attributed to the viscoelastic contrast between the two domains.

Atomic force microscopy (AFM) of rubbed films confirmed the TEM observations. AFM phase images of rubbed and annealed thin films of **PTP-9** exhibited terraces characteristic of flat-on lamellae, whose step height could not be determined from the corresponding height images, probably due to the soft nature of the poly(isobutylene) segments (Fig. 6a). By contrast, the phase images of **PTP-19** thin films revealed a pattern of darker and lighter stripes with a periodicity of about 7 nm, presumably originating from the phase-segregated ''harder'' triad cores and the ''softer'' polymer segments exposed to the surface in the case of vertically oriented lamellae (Fig. 6b).

Electron diffraction of the aligned thin films allowed us to obtain more insight into the molecular arrangement within the layers although a clear-cut picture of the relative orientation of quaterthiophene and perylene blocks could not be obtained

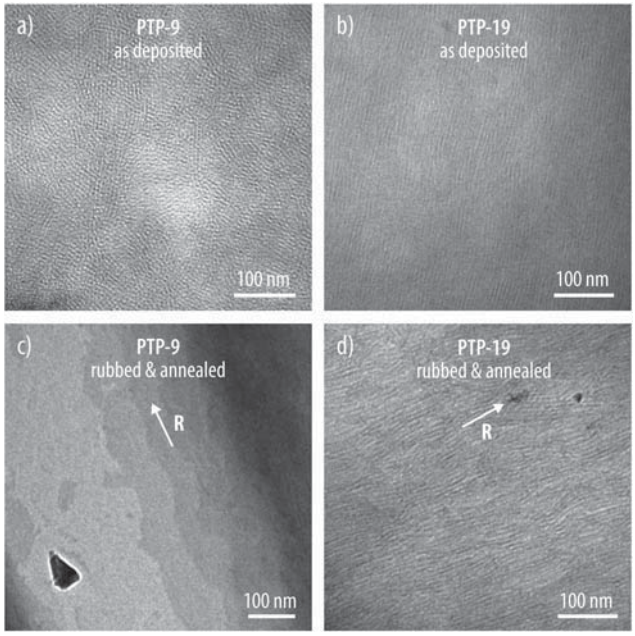

Fig. 5 Transmission electron microscopy images of thin film samples of **PTP-9** and **PTP-19** revealing stripes or terraces that are attributed to lamellae oriented edge-on or face-on relative to the substrate. (a) Films of **PTP-9** deposited by doctor-blading revealed stripes with a periodicity of about 7 nm. (b) Doctor-bladed films of **PTP-19** showing a higher degree of long range order. (c) Upon rubbing and annealing films of **PTP-9**, the lamellae changed their orientation to a face-on orientation, resulting in terraces (annealing temperature 300 °C). (d) This reorientation did not occur for **PTP-19** with longer side chains, which still showed stripes aligned by the rubbing process (annealing temperature 270 °C). The rubbing direction *R* is indicated by the white arrow.

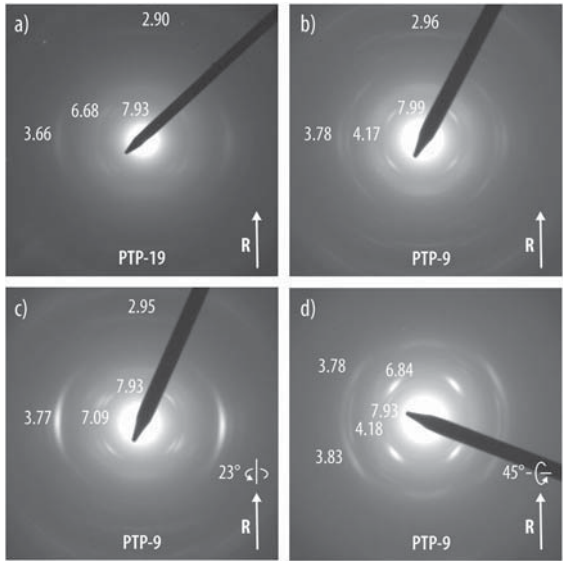

Fig. 7 Electron diffraction patterns of aligned films (annealed at 300 °C) obtained by high-temperature rubbing. (a) **PTP-19** showing reflections at 7.93, 6.68, and 3.66 Å corroborating the distances observed in X-ray diffraction. This pattern is characteristic of standing lamellae. (b) The diffraction pattern of **PTP-9** is dominated by a set of sharp reflections characteristic of the flat-on lamellae. The most intense reflection is observed at 7.99 Å. (c) The diffraction pattern obtained by tilting the **PTP-9** sample grid by an angle of ±23° around the rubbing axis *R* shows the intense 3.77 Å reflection corresponding to the π-stacking distance between triad molecules. (d) The diffraction pattern obtained by tilting the **PTP-9** sample grid by an angle of ±45° around the axis perpendicular to the rubbing axis *R* shows two bands at around 3.8 Å.

because of a limited set of reflections (Fig. 7). All diffraction patterns appeared sharper for **PTP-9** with shorter side chains, which indicated a higher level of crystalline order as compared to **PTP-19** thin films. In agreement with the distances obtained from XRD, **PTP-19** showed reflections corresponding to distances of d = 7.93, 6.68, and 3.66 Å, the latter being close to the π–π stacking distance observed for perylenes. **PTP-19** always showed lamellae more or less normal to the substrate irrespective of the annealing temperature. Instead, for **PTP-9**, changing the annealing temperature from 200 °C to 300 °C resulted in a clear change in the diffraction pattern with the presence of intense reflections at 2.96Å, 3.78 Å and 7.99 Å in films annealed at 300 °C.

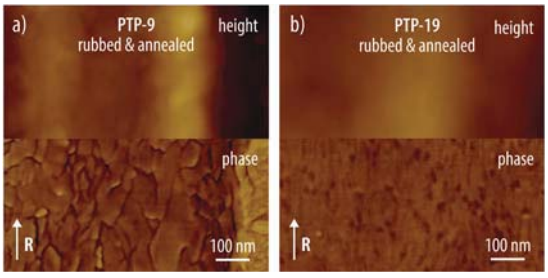

Fig. 6 AFM images confirming that the lamellae are oriented (a) face-on for **PTP-9** and (b) edge-on for **PTP-19**. The rubbing direction *R* is vertical in both cases. Color scale ranges are (a) 140 nm and 90° and (b) 150 nm and 50°.

When tilting the sample by an angle of ±23° (Fig. 7c) around the rubbing direction *R*, the diffraction pattern showed a maximum intensity of the equatorial reflection at 3.77 Å, which corresponds to the π-stacking period between the perylenes and/or quaterthiophene segments (as also observed by XRD, Fig. 4). At the same time, tilting the sample ±45° around the axis perpendicular to the rubbing direction (Fig. 7d) maximized the intensity of the reflections at 6.84 Å. One may conclude that the molecular long axis is tilted 45° relative to the substrate in the rubbing direction, and the π-stacking direction has a component that has a 23° angle relative to the substrate (Fig. 8). At the same time, the molecules must have a small angle ±θ with the lamellar orientation so that their long axes are, on average, oriented parallel to the latter (according to polarized optical microscopy).

Charge generation under illumination

The structural characterization of thin films prepared from **PTP-9** and **PTP-19** showed that both materials form lamellar phases that were macroscopically aligned and retained their ''edge-on'' orientation upon rubbing in the case of **PTP-19**. Since this structure would render the system interesting for charge generation and transport, we proceeded to study excitation and charge transfer processes in these materials in solution and in thin films by means of steady state and TA spectroscopy. To this end, solutions of **PTP-19** in tetrachloroethane (TCE; c = 10 μmol L^{-1}) thermally equilibrated at 100 °C for 1 min, as well as solutions

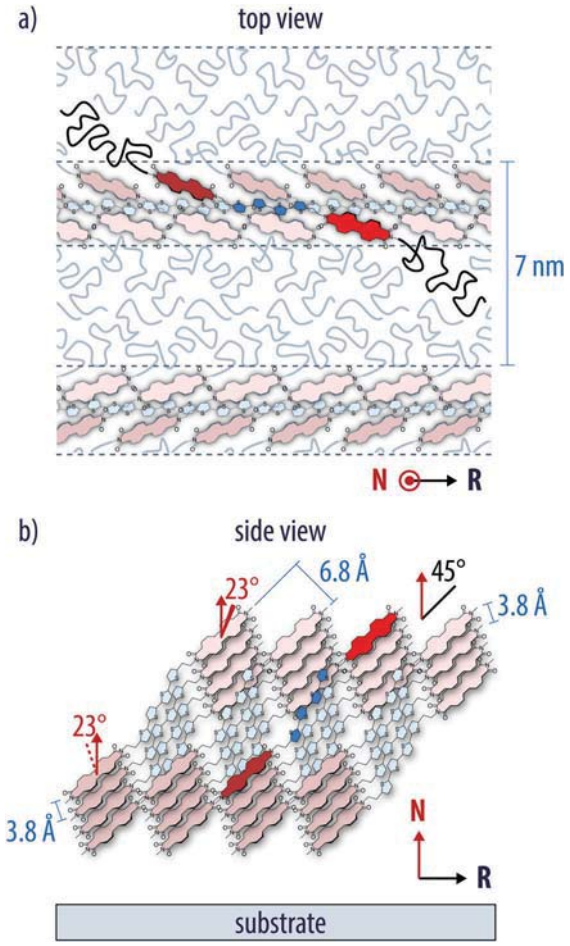

Fig. 8 Schematic illustration of the molecular packing in the lamellar structure according to electron diffraction; (a) a top view of the lamellae (polymer segments not drawn to scale), (b) side view of the triad in a lamella (attached polymer segments omitted for clarity); the triad cores are, on average, aligned with their long axes parallel to the rubbing direction *R*; according to the ED experiments with a tilting stage, they have an inclination of 45° relative to the direction normal to the substrate *N*, and the π-conjugated planes (supposedly, of the perylenes) have an angle of ±23° relative to *N* in a plane perpendicular to *R*.

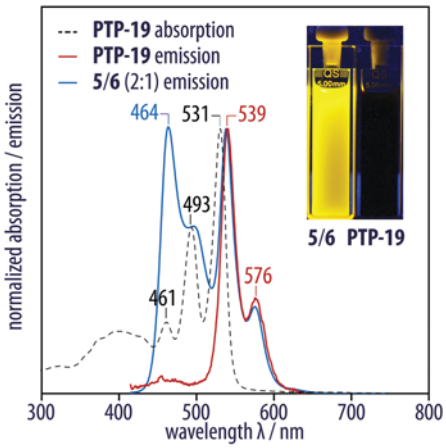

Fig. 9 The emission spectrum (upon excitation at 400 nm) of **PTP-19** (red) is identical to the emission of perylene **5** (not shown). However, compared to the mixture **5**/**6** (2 : 1) with the same composition of the individual chromophores (blue), fluorescence is quenched by more than 99% (inset). In comparison with the mixture, the absence of the quaterthiophene emission feature in the emission of the triad **PTP-19** suggests energy transfer to the perylene moiety.

of a mixture of the reference compounds **5**/**6** (2 : 1) at the same concentration of chromophores, remained molecularly dispersed for several hours at room temperature, according to UV/vis spectroscopy (Fig. 9). However, while the emission spectrum of the mixture at an excitation wavelength of 400 nm was a superposition of the spectra of the two chromophores, the emission spectrum of **PTP-19** resembled the emission of perylene bisimide alone, but with its intensity quenched by 99%. The absence of any quaterthiophene emission feature in the emission spectrum of **PTP-19** suggests an efficient energy transfer from quaterthiophene to the perylene moiety, while the strong quenching of the perylene bisimide fluorescence is an indication of a subsequent charge transfer.

In order to verify this hypothesis, TA spectroscopy was performed on the triad **PTP-19**, individual reference molecules **5** and **6** and their mixture **5**/**6** (2 : 1), both in molecularly dispersed solutions in TCE and in thin films (see Fig. S3, ESI†).

Since the absorption bands of the two chromophores in the solution-phase spectra were well separated, the perylene bisimide moieties could be exclusively excited at 530 nm, while mostly the quaterthiophene chromophores were excited at 390 nm. Exciting the perylene bisimide **5** or the mixture **5**/**6** (2 : 1) at 530 nm yielded identical TA spectra showing the ground state bleaching of perylene bisimide, its stimulated emission, and the absorption of its S_1 excited state (710 nm), whose lifetime exceeded the experimentally accessible time window of 1 ns (Fig. 10a and Fig. S4, ESI†). Similarly, the TA spectra of the mixture **5**/**6** (2 : 1) excited at 390 nm were comparable to those of the pure quaterthiophene **6**, as they showed the transition of the excited quaterthiophene from the singlet state (absorbing around 706 nm) to the triplet state (absorbing at 617 nm) with a time constant of 400 ps, in addition to the TA features of perylene bisimide **5** that also weakly absorbs at 390 nm (Fig. 10b and Fig. S4, ESI†). Thus, one can conclude that the quaterthiophene and the perylene bisimide chromophores do not exert an influence on their respective TA spectra at the employed concentration (c = 10 μmol L^{-1}), when they are not covalently linked.

By contrast, the initially populated S_1 state of the perylene bisimide moiety was quenched within a few picoseconds in the case of the triad **PTP-19** excited at 530 nm (Fig. 10c). After an initial weak decay of the S_1 spectral features on the 0.1 ps timescale (Fig. 10e), we observed a decrease of the stimulated emission that was associated with the rise of two new bands at 690 and 717 nm, which can be attributed to the quaterthiophene radical cation and the perylene radical anion, respectively.[36,37] Afterwards, the ground state bleaching of perylene bisimide and both peaks of the charged species decreased to zero. It can be concluded that charge separation occurred by hole transfer from the S_1 state of the perylene bisimide to the quaterthiophene, followed by charge recombination. The two processes were correlated to time constants of 5 and 27 ps, respectively, as deduced from multi-exponential global analysis (Fig. 10e). It should be noted

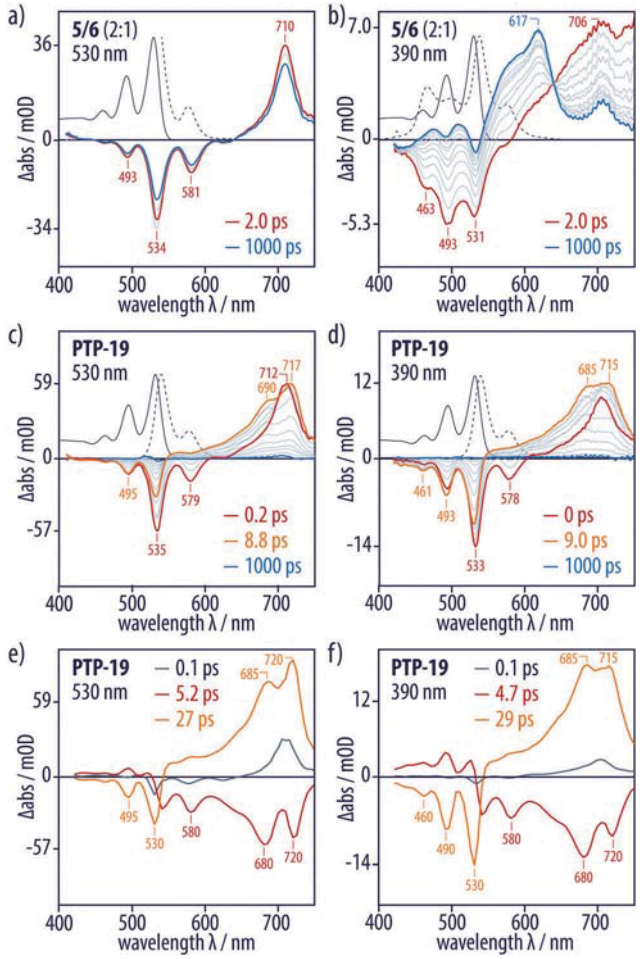

Fig. 10 Transient absorption spectra of the triad **PTP-19** in solution revealing charge separation and recombination upon light absorption. (a) TA spectra of the mixture **5**/**6** (2 : 1) excited at 530 nm show the typical ground state bleaching, stimulated emission, and S_1 photoinduced absorption of the perylene bisimide without any influence of quaterthiophene **6**. (b) TA spectra of **5**/**6** (2 : 1) excited at 390 nm showing quaterthiophene in the S_1 state, which evolves to the triplet state with a time constant of 400 ps, as well as an additional contribution from the perylene in the S_1 state since it weakly absorbs at 390 nm; no influence of the perylene on the excited quaterthiophene is observed. (c) TA spectra of **PTP-19** excited at 530 nm: from perylene in the S_1 state (red) to charged species formed (orange), and recombined to the ground state (blue). (d) TA spectra of **PTP-19** excited at 390 nm are almost identical to (c), showing that energy transfer from quaterthiophene to perylene occurs faster than the resolution of the experimental setup. (e) Multi-exponential global analysis (convolution of a Gaussian IRF with three exponential functions) of **PTP-19** excited at 530 nm correlating with charge separation to a time constant of 5 ps (red) and recombination to a time constant of 27 ps (orange). (f) Multi-exponential global analysis of **PTP-19** excited at 390 nm is almost identical to (e). Absorption and emission spectra of the samples are shown in solid and dashed black lines, respectively.

that a small, long-lived photoabsorption at about 710 nm was observed that was tentatively attributed to small amounts of free perylene bisimide **5** as an impurity in the sample.

Upon excitation at 390 nm, triad **PTP-19** did not exhibit any feature of quaterthiophene in the singlet or triplet state (Fig. 10d). The TA spectra instead revealed only the excited perylene bisimide in the S_1 state, from which charge separation and recombination occurred with similar time constants as after excitation at 530 nm. The relative contribution of the excited perylene bisimide was now significantly larger than in the case of the mixture **5**/**6** excited at 390 nm. Consequently, this contribution in triad **PTP-19** cannot be explained by the weak absorption of the perylene bisimide at 390 nm alone, and suggests an energy transfer from the excited quaterthiophene to the perylene bisimide faster than the time resolution of the experimental setup.

TA measurements were then conducted on thin film samples obtained by drop-casting **5**, **6**, a mixture of **5**/**6** (2 : 1), or **PTP-19** from TCE solutions. As had been the case for the solution-phase samples, the TA spectra of **5** and the mixture **5**/**6** (2 : 1) were identical upon 530 nm excitation, suggesting selective excitation of perylene bisimide in the mixture. These spectra showed the perylene bisimide ground state bleaching in the 420–570 nm region, the stimulated emission at 560 nm, and a broad photo-induced absorption in the region above 600 nm (Fig. 11a and Fig. S4, ESI†). The decay of these three features was associated with the same time constant and was thus correlated.

At an excitation wavelength of 390 nm, the perylene bisimide chromophore was excited more significantly in addition to quaterthiophene, as compared to the solution-phase samples, since the perylene bisimide absorption in the solid-state aggregated form is significantly extended to the blue region. The TA spectra of films of the mixture **5**/**6** (2 : 1) (Fig. 11b) appeared like the superposition of the TA spectra of **5** and **6** excited at the same wavelength (see Fig. S4, ESI†). The ground state bleaching, stimulated emission, and broad photo-induced absorption of perylene were superimposed with the broad photo-induced absorption of the quaterthiophene that featured a maximum at around 700 nm. On the other hand, the TA spectra of triad **PTP-19** excited at either 530 or 390 nm were very similar to one another and showed a different evolution than the reference mixture (Fig. 11c and d). The initially excited state (mainly due to the aggregated perylene bisimides) was characterized by the ground state bleaching below 560 nm, the stimulated emission at 560 nm, and a broad photo-induced absorption with a peak at about 710 nm. While the broad photo-induced absorption certainly had a contribution from the excited perylene-bisimide aggregates, the peak at 710 was reminiscent of the absorption of the charged species in solution and thus was tentatively attributed to charged species in the solid state. The broader aspect of the charge band might be related to higher charge delocalization in the solid state. The initial increase of this charge peak was correlated to a decrease of the stimulated emission, associated with a time constant of 1–2 ps, and attributed to charge separation. It should be noted that the global analysis revealed a simultaneous increase of the ground state bleaching (peaks around 440 and 470 nm) correlated to the same time constant of 1–2 ps (Fig. 11e and f). A possible explanation of this phenomenon would be the migration of excitons or charges to regions where the absorption coefficient of perylene is different due to disorder within the film, which supposedly occurred at a time constant similar to the charge separation. Finally, the decay of the ground state bleaching and the peak at 710 nm were attributed to charge recombination

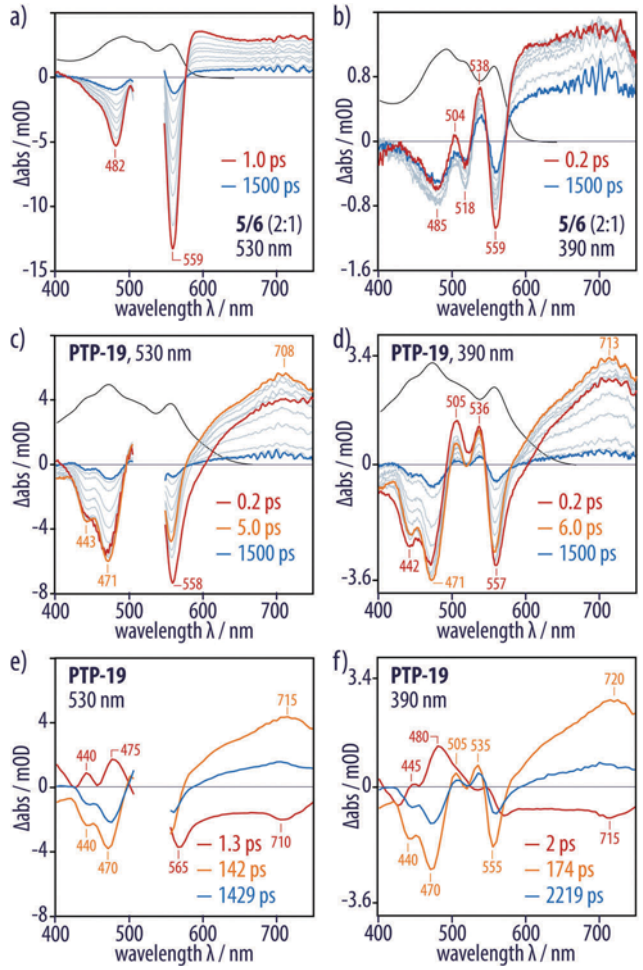

Fig. 11 Transient absorption spectra in thin films of **PTP-19** showing a slower charge recombination than in solution and the formation of long-lived charge carriers. (a) TA spectra of the mixture **5**/**6** (2 : 1) excited at 530 nm are similar to those of perylene **5** alone (Fig. S4, ESI†). (b) TA spectra of **5**/**6** (2 : 1) excited at 390 nm look like a superposition of the spectra of both pure compounds excited at the same wavelength (Fig. S4, ESI†). (c and d) TA spectra of **PTP-19** excited at 530 nm and 390 nm are comparable and show the formation of charged species with a broad absorption peak at around 710 nm. (e and f) Multi-exponential global analysis of **PTP-19** excited at 530 nm and 390 nm reveals that charge separation and recombination occurs with time constants of 1 and 140 ps, respectively; long-lived charge carriers are formed. Absorption spectra of the samples are shown in solid black lines.

occurring with a time constant of about 150 ps according to the global analysis. Different from the solution-phase spectra, however, the system did not completely return to the ground state. Instead, a broad absorption peak at 710 nm persisted on the experiment time scale of 1.5 ns, suggesting the formation of long-lived charge carriers in the thin film samples.

The TA spectra of thin film samples of **PTP-9** were qualitatively identical to those of **PTP-19**. A detailed comparison of the time evolution of the TA intensity at 710 nm, however, showed that the charge-separated species were slightly more long-lived for **PTP-19** than for **PTP-9** (Fig. 12a). While the difference was small, it may still indicate that the higher degree of nanostructural order of **PTP-19** was beneficial for charge delocalization and stabilization.

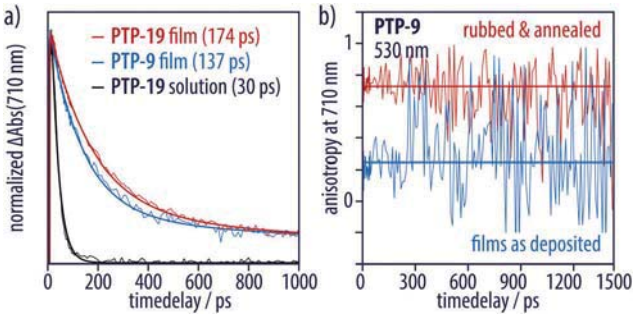

Fig. 12 (a) Comparison of the TA dynamics at 710 nm and the corresponding fit after excitation at 530 nm; recombination is much slower in films compared to solutions, and films made from **PTP-19** show a slower recombination as compared to **PTP-9**. (b) Anisotropy calculated for **PTP-9** at 710 nm after excitation at 530 nm; aligned films show an anisotropy well above those of non-aligned films; the stability of the anisotropy of non-aligned films suggests that charges did not travel between domains within the 1.5 ns timeframe of the experiment.

Furthermore, the anisotropy of the charged species at 710 nm was evaluated on films of **PTP-9** that had been excited at 530 nm (Fig. 12b). As expected, films before alignment by rubbing showed an anisotropy coefficient lower than 0.4, while the aligned films had a coefficient well above it. For the non-aligned film, the anisotropy was stable over the timescale of the experiment, which indicated that the charged species did not travel across domain boundaries and retained their (local) alignment.

In summary, TA spectroscopy confirmed that charge separation occurred in the triads **PTP-9** and **PTP-19** upon light absorption. The initial charge separation process involved the excited state of the perylene bisimide moiety, which could be accessed either by direct excitation or by energy transfer from the excited quaterthiophene moiety. Charge generation was found to be faster and charge recombination slower in thin films as compared to solution-phase samples. The faster charge separation was presumably due to the closer proximity of the chromophores in the solid state, while the slower recombination and especially the formation of long lived charged species was most likely due to the higher stability of charges delocalized within the respective sublayers of the triad lamellae.

Conclusions

We prepared a perylene–quaterthiophene–perylene triad substituted with poly(isobutylene) segments that served to induce the reliable formation of lamellar phases by means of the phase segregation between the rod-like triad core and the attached random coil polymers. In thin films, the triads indeed gave rise to lamellar structures that could then be aligned by rubbing and annealing. The longer side chains of the derivative **PTP-19** helped to increase the long-range nanoscale order and maintain an "edge-on" orientation of the lamellae relative to the substrate after rubbing and annealing. In solution, the fluorescence of the triad **PTP-19** was quenched to more than 99% compared to the mixture **5**/**6** (2 : 1) of the same composition of the chromophores. Transient absorption measurements confirmed that fluorescence

quenching was due to charge separation between the perylene and quaterthiophene moieties, followed by recombination. In thin films, this recombination was slower, and long-lived charged species were observed, presumably due to stabilization through delocalization of the separated charges within the respective sublayers of the triad lamellae. The stable anisotropy factor recorded for nonaligned films suggested that charges did not travel across domain boundaries within 1.5 ns of the experiment. In this way, the higher degree of long-range order in films of **PTP-19** should enhance charge stabilization, and was likely responsible for the even slower charge recombination compared to films of **PTP-9**. An investigation of photovoltaic devices from these materials was beyond the scope of the present study, in particular, because it would have required using a more promising donor segment than the quaterthiophene. Nevertheless, our investigations demonstrate that the terminal attachment of soft polymer segments to a triad system represents a viable concept to prepare triad-based materials with a phase morphology suited for an ordered heterojunction, and that this morphology was beneficial for the stabilization of charge carriers.

Acknowledgements

The authors would like to acknowledge funding from the Swiss National Science Foundation (SNF grants 200020_121812, 200020_144417, and PP00P2_15053), the European Research Council (ERC starting grant 239831), and the Velux Foundation (Velux Projekt 715) as well as financial support from EU interreg Rhin Solar project (C25).

References

1 N. Armaroli and V. Balzani, *Angew. Chem., Int. Ed.*, 2007, **46**, 52–66.
2 O. Morton, *Nature*, 2006, **443**, 19–22.
3 F. Gao and O. Inganas, *Phys. Chem. Chem. Phys.*, 2014, **16**, 20291–20304.
4 J.-L. Brédas, J. E. Norton, J. Cornil and V. Coropceanu, *Acc. Chem. Res.*, 2009, **42**, 1691–1699.
5 T. M. Clarke and J. R. Durrant, *Chem. Rev.*, 2010, **110**, 6736–6767.
6 M. T. Dang, L. Hirsch, G. Wantz and J. D. Wuest, *Chem. Rev.*, 2013, **113**, 3734–3765.
7 M. C. Scharber and N. S. Sariciftci, *Prog. Polym. Sci.*, 2013, **38**, 1929–1940.
8 A. J. Heeger, *Adv. Mater.*, 2013, **26**, 10–28.
9 B. C. Thompson and J. M. J. Fréchet, *Angew. Chem., Int. Ed.*, 2008, **47**, 58–77.
10 P. Westacott, J. R. Tumbleston, S. Shoaee, S. Fearn, J. H. Bannock, J. B. Gilchrist, S. Heutz, J. deMello, M. Heeney, H. Ade, J. Durrant, D. S. McPhail and N. Stingelin, *Energy Environ. Sci.*, 2013, **6**, 2756.
11 S. Sweetnam, K. R. Graham, G. O. Ngongang Ndjawa, T. Heumüller, J. A. Bartelt, T. M. Burke, W. Li, W. You, A. Amassian and M. D. McGehee, *J. Am. Chem. Soc.*, 2014, **136**, 14078–14088.
12 C. Groves, *Energy Environ. Sci.*, 2013, **6**, 1546.
13 A. A. Paraecattil and N. Banerji, *J. Am. Chem. Soc.*, 2014, **136**, 1472–1482.
14 B. Gholamkhass and S. Holdcroft, *Chem. Mater.*, 2010, **22**, 5371–5376.
15 A. Yassar, L. Miozzo, R. Gironda and G. Horowitz, *Prog. Polym. Sci.*, 2013, **38**, 791–844.
16 J. Roncali, *Adv. Energy Mater.*, 2011, **1**, 147–160.
17 L. Dong, W. Li and W.-S. Li, *Nanoscale*, 2011, **3**, 3447.
18 G. Fernández, L. Sánchez, D. Veldman, M. M. Wienk, C. Atienza, D. M. Guldi, R. A. J. Janssen and N. Martin, *J. Org. Chem.*, 2008, **73**, 3189–3196.
19 T. Nishizawa, K. Tajima and K. Hashimoto, *J. Mater. Chem.*, 2007, **17**, 2440.
20 L. Bu, X. Guo, B. Yu, Y. Fu, Y. Qu, Z. Xie, D. Yan, Y. Geng and F. Wang, *Polymer*, 2011, **52**, 4253–4260.
21 L. Bu, X. Guo, B. Yu, Y. Qu, Z. Xie, D. Yan, Y. Geng and F. Wang, *J. Am. Chem. Soc.*, 2009, **131**, 13242–13243.
22 P.-O. Schwartz, L. Biniek, E. Zaborova, B. Heinrich, M. Brinkmann, N. Leclerc and S. Méry, *J. Am. Chem. Soc.*, 2014, **136**, 5981–5992.
23 J. Qu, B. Gao, H. Tian, X. Zhang, Y. Wang, Z. Xie, H. Wang, Y. Geng and F. Wang, *J. Mater. Chem. A*, 2014, **41**, 1086–1097.
24 J. Kelber, H. Bock, O. Thiebaut, E. Grelet and H. Langhals, *Eur. J. Org. Chem.*, 2011, 707–712.
25 C. Xue, R. Sun, R. Annab, D. Abadi and S. Jin, *Tetrahedron Lett.*, 2009, **50**, 853–856.
26 J. Gebers, D. Rolland, R. Marty, S. Suàrez, L. Cervini, R. Scopelliti, J. C. Brauer and H. Frauenrath, *Chem. – Eur. J.*, 2015, **21**, 1542–1553.
27 R. Marty, R. Nigon, D. Leite and H. Frauenrath, *J. Am. Chem. Soc.*, 2014, **136**, 3919–3927.
28 J. Mizuguchi and K. Tojo, *J. Phys. Chem. B*, 2002, **106**, 767–772.
29 T. Tanaka, Y. Chatani and H. Tadokoro, *J. Polym. Sci., Polym. Phys. Ed.*, 1974, **12**, 515–531.
30 J. Gebers, L. Hartmann, B. Ozen, M. Schaer, S. Suàrez, P. Bugnon, R. Scopelliti, H.-G. Steinrück, O. Konovalov, A. Magerl, M. Brinkmann, R. Petraglia, P. de Silva, C. Corminboeuf and H. Frauenrath, In preparation.
31 E. Croisier, S. Liang, T. Schweizer, S. Balog, M. M. cacute, R. Snellings, J. E. L. Cugnoni, V. E. R. Michaud and H. Frauenrath, *Nat. Commun.*, 2014, **5**, 1–10.
32 R. Marty, R. Szilluweit, A. Sánchez-Ferrer, S. Bolisetty, J. Adamcik, R. Mezzenga, E.-C. Spitzner, M. Feifer, S. N. Steinmann, C. Corminboeuf and H. Frauenrath, *ACS Nano*, 2013, **7**, 8498–8508.
33 L. Biniek, P.-O. Schwartz, E. Zaborova, B. Heinrich, N. Leclerc, S. Méry and M. Brinkmann, *J. Mater. Chem. C*, 2015, **3**, 3342–3349.
34 K. I. Winey, S. S. Patel, R. G. Larson and H. Watanabe, *Macromolecules*, 1993, **26**, 2542–2549.
35 K. I. Winey, S. S. Patel, R. G. Larson and H. Watanabe, *Macromolecules*, 1993, **26**, 4373–4375.
36 D. Fichou, G. Horowitz, B. Xu and F. Garnier, *Synth. Met.*, 1990, **39**, 243–259.
37 T. Roland, J. Léonard, G. Hernandez Ramirez, S. Méry, O. Yurchenko, S. Ludwigs and S. Haacke, *Phys. Chem. Chem. Phys.*, 2011, **14**, 273.